Tellus (1989), *41A*, 385–400

On the effects of the damping mechanisms in an atmospheric general circulation model

By LEIF LAURSEN* and ERIK ELIASEN, *Geophysical Institute, Department of Meteorology, University of Copenhagen, Haraldsgade 6, DK-2200 Copenhagen N, Denmark*

(Manuscript received 25 July 1988; in final form 19 January 1989)

ABSTRACT

A version of ECMWF's first spectral model with a comprehensive physical parameterization package has been used for long-term integrations in perpetual January mode. The model has 9 sigma-levels in the vertical and the expansion of the horizontal fields are truncated at total wavenumber $n = 31$. In order to simulate the observed January climate both in terms of mean-fields as well as the spectral distribution of the kinetic energy as accurately as possible, a series of experiments has been performed with varying parameterizations of some physical processes, especially the damping mechanisms. The inclusion of a simple gravity wave drag is found to have a substantial impact on the simulations. The position and depth of the mean sea level quasi-stationary low pressures in the northern hemisphere is more in accordance with their observed counterparts with the gravity wave drag included, and the excessive stratospheric polar night jet, which is developed in the model without the drag, is effectively controlled by this parameterization. The sensitivity due to changes in the vertical diffusion of momentum, heat and moisture has been considered by crude variations in the mixing length. It turns out that even large changes in the value of the mixing length have a quite modest influence on the mean fields simulated by the model. The horizontal diffusion is necessary in order to represent the effect of the unresolved scales on the explicitly predicted scales. The parameterization of this effect is incorporated in the model as a linear term utilizing that in a spectral formulation, a linear diffusion can easily be formulated with any scale dependency. It is found that an increase of the diffusion in the smallest scales may result in an increase of eddy kinetic energy of the larger scales and even an increase in the total eddy kinetic energy. Moreover it appears that it is quite possible to formulate the linear diffusion of the model to simulate the observed spectral variations of kinetic energy for the medium and smaller scales.

1. Introduction

The use of comprehensive atmospheric general circulation models in climate studies has increased considerably in recent years concurrently with the increase of computer resources. A climate modelling project was thus initiated at the Geophysical Institute, University of Copenhagen when the installation of a new computer system at the Danish Meteorological Institute was completed. As discussed for instance by Simmons and Bengtsson (1984), the development in numerical modelling has blurred the distinction between numerical models for climate research and for medium-range weather forecasting. The main difference between the two types of models is the time for which they must be integrated and, depending on that, the degree of spatial resolution being possible. It was therefore found very appropriate to base a medium-resolution climate model on the advanced prediction model developed at the European Centre for Medium Range Weather Forecasts (ECMWF). A version of the ECMWF's spectral model was applied and its spatial resolution adjusted to the computer capacity available and

* Present affiliation: Danish Meteorological Institute, Lyngbyvej 100, DK-2100 Copenhagen Ø, Denmark.

then the model was tested regarding its ability to simulate characteristic features of the general circulation, primarily for January conditions. A number of errors common for other similar models was found, especially a too small eddy kinetic energy, too strong westerlies at the upper levels of the model at the vicinity of the north pole and some shortcomings in the simulation of the stationary planetary waves. It was attempted to remove or at least to diminish these errors by making a number of changes in the model.

In the present paper, we will focus especially on the effects of changing the damping mechanisms in the model not from the point of view of short- or medium-range forecasting, but merely by considering the impact on the long-term balance determining the general circulation. The vertical diffusion is a principal damping mechanism associated with the vertical transfer of momentum, heat and moisture by small-scale turbulent eddies. In general circulation models with several levels, the vertical diffusion is represented by a unified formulation embracing the exchange between the surface and the atmosphere, the boundary layer and the possible turbulent transfer in the free atmosphere. It has not been the intention to study the effects of more-or-less sophisticated parameterizations of vertical diffusion, but only to consider the sensitivity of the model to crude variations of the strength of the vertical diffusion as expressed by the mixing length. It turns out that even large changes in the value of the mixing length have a quite modest influence on the mean fields simulated by the present model. Another parameterization associated with the vertical transfer of momentum, namely that of a gravity wave drag, has on the other hand a significant impact on the general circulation. During the last few years, more-or-less advanced representations of the sub-grid scale vertical momentum transport by mountain gravity waves have been introduced in several general circulation models. In the present work, the effect of the gravity wave drag has been considered by using a very simple formulation. In Section 3, the impact of this parameterization on the simulation is demonstrated.

A further damping mechanism used in all general circulation models is lateral diffusion. Using a spectral model, it is not necessary to introduce any lateral diffusion in order to prevent numerical instability in calculation of the non-linear terms. It is necessary, however, to incorporate a suitable form of diffusion as representing the effect of unresolved scales on the explicitly predicted scales. Unfortunately, the physical mechanism underlying this effect is not fully understood, so its parameterization must rely mainly on heuristic arguments. A numerical integration with a model without any lateral diffusion term will quite soon become unrealistic due to an accumulation of kinetic energy on the small components near the truncation limit. Thus, the effect of the lateral diffusion term must be to prevent this so-called spectral blocking and more generally to ensure realistic spectral distributions of energy. Simultaneously with the change from a horizontal grid-point representation to a spectral representation which has taken place in most global models, it was found computationally suitable to simplify the formulation of the lateral diffusion by a linear term, and thereby utilizing that in the spectral formulation a linear diffusion can quite easily be formulated with any scale dependency for each spectral component. By experimentation with the present model, it was considered appropriate to study how changes of the scale dependency as well as the strength of the lateral diffusion will influence the simulated general circulation, especially in relation to the systematic errors of the model. In Section 4, the results concerning the kinetic energy and its spectral distribution will be presented. It is found that an increase of diffusion on the smallest scales may result in an increase of eddy kinetic energy of the larger scales and even an increase of the total eddy kinetic energy. Moreover, it appears that it is quite possible to formulate the linear diffusion in such a way that the model simulates the observed spectral variation of kinetic energy for the medium and smaller scales.

2. The model

The model used for the experiments presented in this paper is based on the first spectral forecast model developed at ECMWF (Baede et al., 1979). The prognostic variables describing the horizontal motion are the vorticity and divergence of the horizontal wind. The mass continuity equation in vertically integrated form is used as prognostic equation for the logarithm of surface pressure and as diagnostic equation for the derivative of sigma with respect to time. The thermodynamic equation is used for prediction of virtual temperature and finally the continuity equation for water vapor mixing ratio completes the system of prognostic equations. The horizontal representations of the dependent variables are truncated series of spherical harmonics with zonal wavenumber m and total wavenumber n (the order of the Legendre polynomials), and the model employs the transform method (Eliasen et al., 1970; Orszag, 1970). The model was developed for medium-range weather forecasting, and it has been used with varying horizontal resolution for this purpose at ECMWF. The truncation has been chosen to be triangular and the maximum total wavenumber n is used to express the horizontal resolution, so TN is used for a truncation at $n = N$. The horizontal resolutions considered at ECMWF have been T21, T42, T63 and T106. The generally satisfactory behavior of the low-resolution spectral model T21 has led it to be used for long-term integrations as for instance by Volmer et al. (1984), Cubasch (1985) and more recently for climate simulations at the Hamburg Climate Computing Centre (Fischer, 1987). Certainly it is quite likely that a higher spatial resolution should be used in order to obtain a satisfactory description of the different physical processes, so in order to approach the higher horizontal resolutions without a too large increase in computer resources needed, it was decided to use the model as T31. With this resolution, the model may be considered as a low-resolution model compared with models used for deterministic weather forecasting, but compared with models generally used for long-term integrations or climate studies, T31 is a quite high horizontal resolution. For the T31 representation, the physical processes are computed in the transform grid with 48 Gaussian latitudes and 96 equally spaced longitude points. The vertical coordinate in the model is sigma, equal to pressure normalized with its surface value. At ECMWF, the model was used with 15 levels with the values of sigma given by a 4th-order polynomial in the level number. For the present application, the number of levels has been reduced to 9, but the vertical spacing of sigma layers is obtained from the same 4th-order polynomial giving the following values at full levels carrying the prognostic variables: 0.042, 0.132, 0.237, 0.360, 0.500, 0.648, 0.792, 0.914 and 0.989. The semi-implicit time-stepping scheme is used together with a weak time filter, and the time-step used is 30 min. With this choice of spatial resolution and time-stepping scheme, the model can be integrated over 1 month in 35 min on the available AMDAHL VP1100 computer.

Sources and sinks of energy due to solar and thermal radiation are calculated on the basis of the two-stream approximation as it has been developed by Geleyn and Hollingsworth (1979). The short-wave and long-wave part of the spectrum are divided into 2 and 3 subintervals, respectively, for which calculations are done separately. The scheme in the form used here generates its own clouds from relative humidity, whereas ozone, carbon dioxide and aerosols are prescribed with their observed contents and spatial variations. This comprehensive radiation scheme is rather computer demanding, so the simulation of the diurnal cycle is not considered and furthermore, the interval between the application of the scheme is chosen to be 24 h.

The parameterization of deep convection in the models used at ECMWF has been based on the Kuo-scheme as described by Tiedtke et al. (1979). The introduction of the parameterization of shallow non-precipitating convection has been shown to have a positive impact on the hydrological cycle and consequently on the diabatic heating in the operational model at ECMWF (Tiedtke, 1985). The inclusion of a similar formulation of shallow convection in the present model is dubious, considering its coarser vertical resolution. Recently, a new convective scheme has been proposed by Betts (1986), which includes parameterization of both deep and shallow convection, and this scheme has been adapted to the present model. The scheme utilizes the concept of quasi-equilibrium between cloud fields and synoptic scale conditions and parameterizes the changes of heat and moisture by simultaneously adjusting the model profiles towards observational-based reference profiles, which implies that in convective situations, the thermal structure of the model will be forced towards observed climatology. The reference profiles are determined for each grid point every time-step, with stability and humidity structures depending on the type of convection. The cloud-top height found using the moist adiabat from the lowest level distinguishes shallow and deep convection. In the present model, the convection is assumed to be shallow if the cloud top is below level 6 (about 650 hPa). The adjustment rate used is 2 h for both shallow and deep convection. Other details about the scheme follow the work by Betts (1986) and Betts and Miller (1986). The large-scale precipitation scheme, which is employed after the convective adjustment scheme, is used in the form described by Tiedtke et al. (1979).

Over the oceans, the surface temperature is fixed to its climatological value, and the surface stress is determined using the formula by Charnock (1955). For temperatures below $-2°C$, sea-ice is assumed with increased albedo and decreased values for the roughness length. Over land, the surface temperature is a prognostic variable, but it is linked through a diffusion term to a climatological deep soil temperature, whereas the roughness length is prescribed. The vertical fluxes of momentum, sensible heat and latent heat at the surface-atmosphere interface are dependent on the stability and roughness length (Monin-Obukhov). Above the lowest layer, the turbulent fluxes are determined by the mixing length scheme as has been formulated by Louis (1979). The diffusion coefficients depend in this formulation largely on the mixing length. The profile of the mixing length is determined by the formula proposed by Blackadar (1962) describing the increase from below to some fixed asymptotic mixing length. In most experiments considered here, the mixing length has been chosen to be 100 m for all three kinds of fluxes, but also some experiments with varying values of the mixing length have been performed.

The effect of orography enters the model equations directly through the specification of the geopotential height at the surface. This geopotential height is necessarily very smooth in general circulation models. The concept of enhanced or envelope orography was introduced by Wallace et al. (1983) in order to reduce systematic errors due to insufficient orographical forcing in the ECMWF (T63) forecast model. The effect of envelope orography has been the subject of an investigation concerning its dependence on model resolution, Jarraud et al. (1985), where it turned out that for a low-resolution model (T21), the impact on the models error features of using an envelope orography, was little or even negative. Hence, the envelope orography has not been considered in the present model. However, a significant effect of orography is associated with gravity waves generated over sub-grid scale orographical features. These waves may propagate upward to high levels, where they are absorbed or dissipated. Although the possibility that gravity wave activity may have an important impact on the large-scale flow was suggested many years ago (Lilly, 1972), the parameterization of gravity wave drag in general circulation models is quite new (Boer et al., 1984; Dickinson, 1985; Palmer et al. 1986). In the present model, the mean orography is used together with a very simple but efficient parameterization of gravity wave drag following the formulation described by Dickinson (1985). The effect of gravity wave drag enters the tendency equation for the zonal component of the wind as

$$\frac{\partial u}{\partial t} = -\frac{g}{p_*}\frac{\partial \tau_x}{\partial \sigma}, \tag{1}$$

where u is the zonal component of the horizontal windvector, g is the acceleration of gravity, p_* the surface pressure and τ_x is the stress in zonal direction due to gravity wave motion. At the surface, this stress is assumed to be given by the expression

$$\tau_{sx} = k\rho u N h'^2, \tag{2}$$

where k is a constant, ρ and N are the density and Brunt-Väisälä frequency at low altitude, respectively. The quantity h'^2 is the variance of the sub-gridscale orography. Eq. (2) is further simplified to

$$\tau_{sx} = \lambda p_* u_8(\Theta_7 - \Theta_9)^{1/2} h'^2, \tag{3}$$

where the indices refer to model levels counted from above. Θ is the potential temperature and λ is a constant with the value $1.275 \cdot 10^{-12}$ $s\,m^{-3}\,K^{-1/2}$ normally used in the present model. Similar equations are applied for the meridional component. The variance h'^2 is determined from a high-resolution orographic dataset (US Navy), and it is limited to $(400\text{ m})^2$ in order to avoid too excessive stress at the edges of the mountain ranges. The vertical variation of the stress is treated in the most simple way by assuming it to be constant in the lowest 3 layers of the model (up to about 720 hPa) from where it decreases linearly with sigma to zero at the top of the atmosphere or at the level where the wind component under consideration changes sign compared to its low-level value.

The lateral diffusion is taken into account in the model by the analogous expressions in the equations for vorticity, divergence, virtual temperature and humidity. Formally, the vorticity equation may be written

$$\frac{\partial \xi_{m,n}}{\partial t} = R_{m,n} + F_{m,n}, \tag{4}$$

where $\xi_{m,n}$ is the spectral component of the vorticity with m and n representing the zonal and total wavenumber, respectively. $F_{m,n}$ represents the lateral diffusion and $R_{m,n}$ all other terms. In several spectral models (for instance the models at ECMWF), the expression

$$F_{m,n} = -J\nabla^4 \xi_{m,n} = -Ja^{-4} n^2(n+1)^2 \xi_{m,n} \tag{5}$$

is used with J being a constant. Generally, the scale dependency in terms of the spectral total wavenumber n may be written

$$F_{m,n} = -L_n \xi_{m,n}, \tag{6}$$

where L_n is a function increasing more-or-less with n. In order to have the possibility to increase the damping on the smaller scales of motion in the spectral representation without a simultaneous increase of damping of the larger scales, the following form of L_n may be considered

$$L_n = \begin{cases} L\left(\dfrac{n-n_*}{N}\right)^\beta & n > n_* \\ 0 & n \leqslant n_* \end{cases}, \tag{7}$$

where N is the upper limit of n and L; n_* and β are constants. A lateral diffusion expressed by (7) was introduced in the model of the Canadian Climate Centre described by Boer et al. (1984) on the basis of theoretical considerations, Leith (1971), and with the value of L obtained from the observational study of Chen and Wiin-Nielsen (1978). Both expressions (5) and (6) have been applied in order to investigate the influence of different scale dependency and the influence of the strength has been considered by using different values of L and J including also the value zero. Applying the formulation (7), the values $\beta = 2$ and $n_* = 23$ have been used and L is normally assigned the value $5 \cdot 10^{-4}\,\mathrm{s}^{-1}$. From a theoretical point of view, the effect of the scale selectivity of a linear horizontal diffusion on the development of baroclinic waves in an adiabatic spectral model with a climatological basic state has been studied by MacVean (1983). In view of the quite heuristic arguments concerning the lateral diffusion, it seems quite likely that the optimum diffusion formulation in a general circulation model will depend upon the model itself, both regarding the spatial resolution of the model and the parameterizations used for the different physical processes.

In the numerical integrations, the linear diffusion term is included as an implicit term; thus with τ indicating the number of time steps of length Δt, eq. (4) with (6) may be written

$$\frac{\xi_{m,n}^{\tau+1} - \xi_{m,n}^{\tau-1}}{2\Delta t} = R_{m,n}^{\tau} - L_n \xi_{m,n}^{\tau+1},$$

giving

$$\xi_{m,n}^{\tau+1} = \frac{\xi_{m,n}^{\tau-1} + 2\Delta t R_{m,n}^{\tau}}{1 + 2\Delta t L_n},$$

showing that the diffusive effect is included by multiplying the result of the time-stepping forward, without dissipation, by the factor $(1 + 2\Delta t L_n)^{-1}$.

3. Simulation of January climate

The simulation of the January climate obtained with the version of the model described in the previous section will be considered as a reference for further numerical experiments. In the following, this reference simulation will be compared with the observed climate by considering long-term mean-fields of the general circulation. The statistics of the reference simulation is obtained from a 600-day integration with an arbitrary chosen initial state, namely that with the initial data from the ECMWF analysis of the 15 January 1982. The integration is carried out as a perpetual January simulation, i.e., with constant solar insolation of 15 January and sea surface temperatures and deep soil temperature in land surfaces prescribed as the climatological values for January. Similar perpetual January simulations have been presented for recent years, e.g., for the NCAR community climate model described by Pitcher et al. (1983). It is perhaps questionable to what extent such a perpetual January simulation should actually coincide with observed climate, and in fact it is stated by Zwiers and Boer (1987) for the model of the Canadian Climate Centre that the simulated climate obtained with a perpetual January forcing is significantly different from that obtained with annual cycle forcing. In any case, it must be reasonable to assume that at least the basic features of the simulated perpetual January climate may be tested against the observed climate values.

From several integrations, it was found that an integration of up to 60 days is necessary to have the influence of the initial state removed from the model's own climate and hence to have stationary long-term statistics. Thus, the first 60 days of each integration have been disregarded, and for the following days of the integration, mean values are obtained for periods of 90 days. For the reference simulation, the mean values of 6 such 90-day averages was examined and it was found that the differences from one period to another were quite small compared to the corresponding differences between the reference simulation and the simulations from the considered integrations of the model.

The zonally averaged cross-sections of temperature and zonal wind are shown in Fig. 1 as mean values for the period 60–150 days of the reference integration. For a comparison, Fig. 2 shows the same cross-section for the observed mean of January 1983 computed from the ECMWF analysis. It is seen that the model is reasonably good in simulating the observed tropospheric wind distribution for a single month, and the same will be the case for a comparison with climatological values of the zonal wind. The main difficulty by simulating the mean zonal wind as well as the temperature field occurs in the stratosphere.

The mean sea-level pressure (or 1000 hPa geopotential height) is a fundamental climatological parameter representing the integrated effect of the basic dynamics and thermodynamics of the atmosphere. As a matter of fact, the mean sea-level pressure field has been shown to be quite

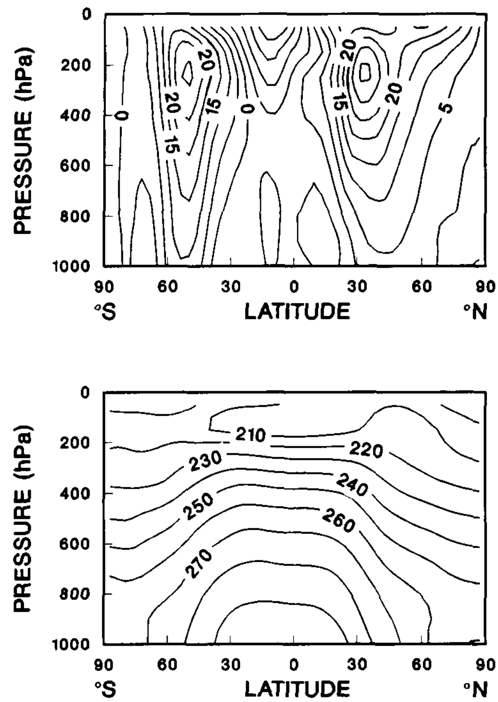

Fig. 1. Time-averaged zonal mean values of the latitude-pressure cross-section of zonal wind (m s^{-1}) and temperature (K) for the reference simulation.

difficult to simulate satisfactorily, and as will be shown later, this field is quite sensitive to changes in the model formulation. Fig. 3 shows the mean 1000 hPa geopotential height for the reference simulation over the northern hemisphere with mean values again taken over the 60–150 day period of integration. For comparison, the observed mean field for three January months 1983, 1984 and 1985 is shown in Fig. 4. As the observed January mean field is known to vary a good deal from one year to another, the 3-year mean will not be climatologically representative, but nevertheless, the well-known main features of the sea-level pressure field is represented quite well by Fig. 4 just as it is simulated quite well by the model integration. In a similar way, the mean geopotential heights in the troposphere are also simulated reasonably well as illustrated by Figs. 5, 6, showing the simulated and observed 500 hPa surface, respectively.

A further very important question about the reliability of the simulation is how well the eddy

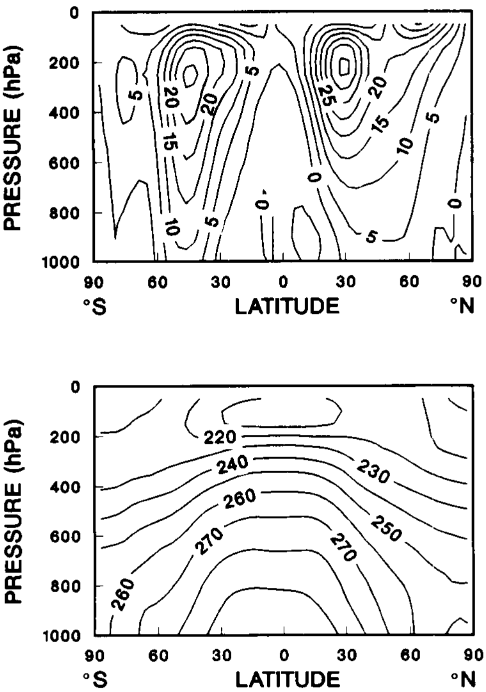

Fig. 2. As Fig. 1, but for January 1983 as derived from ECMWF analysis.

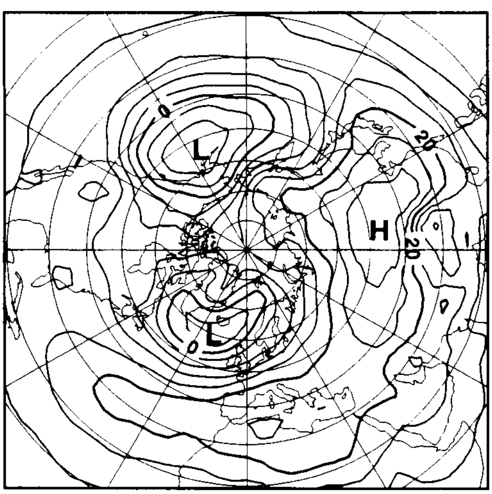

Fig. 3. Time-average of the geopotential height of the 1000 hPa level for the reference simulation. The contour interval is 4 dm.

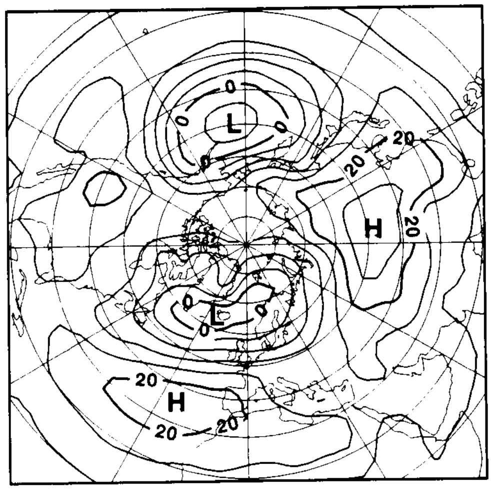

Fig. 4. As Fig. 3, but averaged for the three January 1983, 1984 and 1985 as derived from ECMWF analysis.

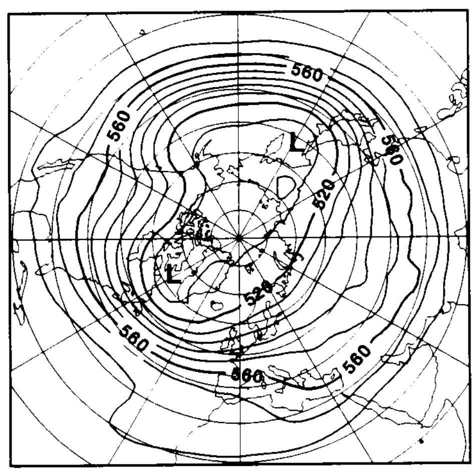

Fig. 5. Same as Fig. 3, but for the 500 hPa level.

activity is simulated, both concerning the intensity and geographical distribution. As the most immediate statistical quantity describing the eddy activity, the temporal standard deviation at the 500 hPa height for 600 days of the reference simulation is shown in Fig. 7 for the northern hemisphere. The corresponding observed standard deviation field for a month varies strongly from one year to another, so in order to have a climatological representative field, it will be necessary to apply mean values over many years.

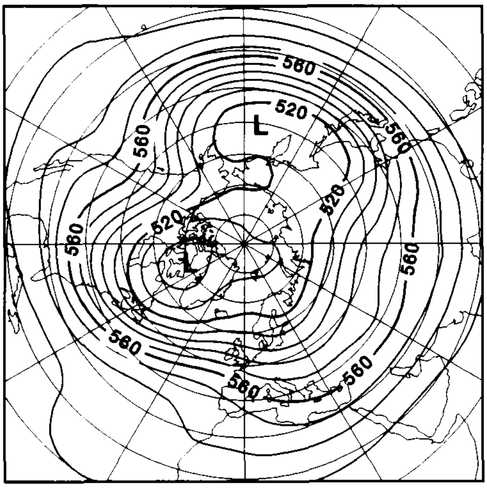

Fig. 6. Same as Fig. 4, but for the 500 hPa level.

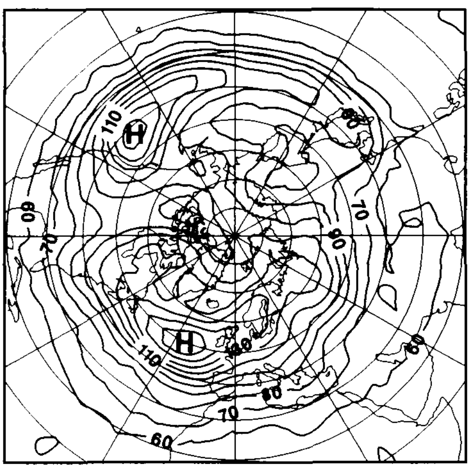

Fig. 7. The temporal standard deviation of the 500 hPa geopotential height for the 600 days of the reference simulation. The contour interval is 10 m.

In the paper by Blackmon et al. (1986), Fig. 2c shows the standard deviation of the 500 hPa height for observations through 60 winter months. From Fig. 7, it is seen that the maxima of the standard deviation field are associated with the Icelandic and Aleutian low-pressure centers. Compared with the observed field, the simulated values are slightly to small and furthermore, the maximum areas occur at more southerly latitudes. A further maximum in the observations over northern Eurasia is not simulated well by the model.

The parameterization of the drag due to orographically-induced gravity waves was included in the reference simulation. The effect of the gravity wave drag in the present model is illustrated in Fig. 8, where the cross-sections of zonally averaged temperatures and zonal velocities are shown for an integration without gravity wave drag. By comparison with Fig. 1, it is obvious that the momentum sink introduced by the gravity wave drag has a large impact on the momentum balance in the stratosphere. Besides the excessive strong polar night jet, too strong winds are also present in the lower troposphere; thus the zonally averaged surface wind in the latitude belt from 40° to 60° north is above 5 m s^{-1}. On the southern hemisphere, the impact of the gravity wave drag is much less pronounced as should be expected. On the northern hemisphere, the gravity wave drag also has a positive

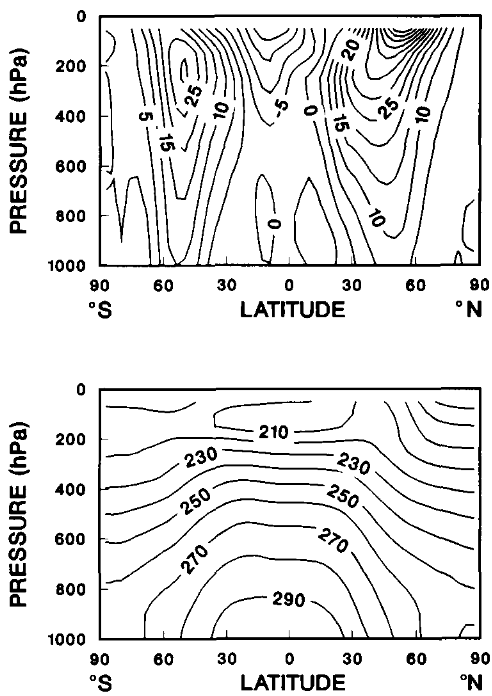

Fig. 8. As Fig. 1, but for the experiment without gravity wave drag.

impact on the standing eddies as may be seen by comparing the 1000 hPa geopotential heights in Fig. 9 with the same quantity in Fig. 3 for the reference simulation. As seen, the North Atlantic low is far too deep and shifted towards the northeast in the integration without gravity wave drag. Similar results were obtained by Boer et al. (1984) and Palmer et al. (1986).

The excessive polar night jet as it appears in Fig. 8 has been a common failure for general circulation models. In the NCAR community climate model, a similar bias was reduced by a careful parameterization of long-wave radiation (Ramanathan et al., 1983). In that model, on the other hand, horizontal diffusion also plays an important rôle in diminishing the extreme stratospheric westerlies (Boville, 1984). Another method for reduction of the polar night jet is to use a linear damping in the momentum equation (Rayleigh friction). Some experiments with the present model using Rayleigh friction in the uppermost 2 levels with varying values of the friction coefficient show that it is quite possible to considerably reduce the bias in the upper-level zonal wind and temperature. However, the effect of this procedure is insignificant in low altitudes where the wind speed remains too strong, reflecting errors in the mean sea-level pressure pattern as in Fig. 9. The use of Rayleigh friction

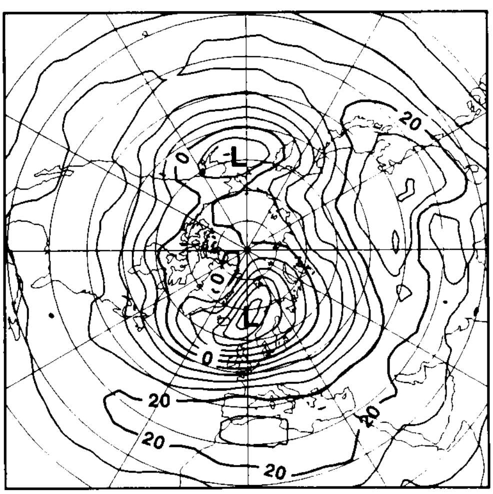

Fig. 9. As Fig. 3, but for the experiment without gravity wave drag.

or enhanced diffusion may be considered as useful numerical tools with little or no physical basis. The gravity wave parameterization on the other hand is based on observed physical phenomena, and moreover, it has a positive impact on the simulation both at high and low levels. It is quite possible that part of the defects visible in the integration without gravity wave drag may be due to inaccuracy in other processes in the model. In the present model, the gravity wave drag formulation has been used both as a physical process in its own right and as a tuning tool. Thus the coefficient λ in eq. (3) is selected in order to optimize the performance of the reference simulation, but the resulting stress is still within the somewhat uncertain limits which, e.g., is summarized in Palmer et al. (1986). The influence of the value used for λ has been considered by an experiment with the value of λ reduced to half its value in the reference experiment. The mean 1000 hPa height field obtained in this experiment is more in accordance with that in Fig. 3 than that in Fig. 9, indicating that the effect of the gravity wave drag parameterization is by no means linear in λ.

The vertical diffusion in the atmosphere above the boundary layer is another damping mechanism which may be considered as being important for the simulated mean fields. Three experiments have been performed which all may be compared with the reference simulation, since the only deviation from this is the change in the vertical diffusion. The most radical is of course to remove the vertical diffusion above the boundary layer. This has been done by performing an experiment with the formulation applied only in the three lowest layers and simultaneously reducing the asymptotic mixing length to 30 m. In the second and third experiments in this category, the vertical diffusion is active at all levels as in the reference experiment with asymptotic mixing lengths equal to 30 and 300 m, respectively. The results of these experiments are equivocal in the sense that it is impossible to find a significant response of the long-term mean fields to the change in the vertical diffusion. The amount of eddy kinetic energy of the smallest scales in the upper troposphere is the only quantity for which a clear signal is seen. The increased values of the mixing length have a marked tendency of reducing the kinetic energy level in these scales, whereas there is hardly any effect on the larger scales.

4. Simulation of the kinetic energy

It is a basic requirement of a general circulation model that it must be able to reproduce the observed amount of kinetic energy both as regards its spatial and spectral distribution. Table 1 shows the principal figures for the whole sphere of the mean kinetic energy at the 500 hPa level for the 450–600 days of the reference simulation and for the observed values for the three January months 1983–1985. Conventionally, the total kinetic energy is divided into the kinetic energy of the zonal flow KZ and the energy of the eddy motions KE and furthermore into the energy of the stationary motion and the transient motions. It is a well-known defect by most general circulation models that they reproduce a somewhat too small eddy kinetic energy, and from Table 1, it is seen that the value of the simulated KE actually is about 80% of the observed value. In the lower part of the troposphere, the simulated KE is about 90% of observed value, whereas at the 250 hPa level, the simulated value is only 70% of the observed one. The values listed in Table 1 are computed from the rotational part of the velocity field. The corresponding values for the divergent part of the motion are as expected quite small, about 3% of the total eddy kinetic energy. The meridional and vertical distribution of the kinetic energy of the stationary zonal mean flow may of course be deduced from the cross-sections shown in Fig. 1. The geographical distribution of the eddy kinetic energy is broadly connected with the horizontal field of the standard deviation of the height field as shown in Fig. 7. More precisely, Fig. 10 shows the meridional variation of the kinetic energy for the total (upper part) as well as

Table 1. *Kinetic energy at 500 hPa* ($m^2\ s^{-2}$)

	Simulated		Observed	
	KZ	KE	KZ	KE
standing	55.2	15.9	63.9	18.7
transient	2.1	45.4	3.6	57.0

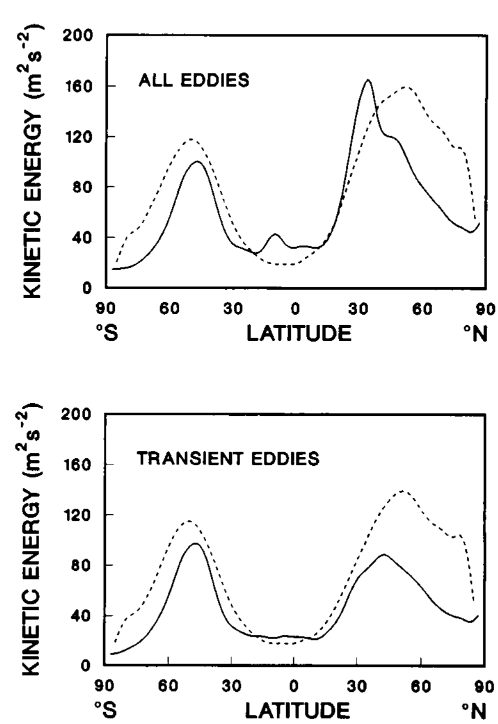

Fig. 10. The meridional variation of the eddy kinetic energy ($m^2\ s^{-2}$) at the 500 hPa level. The upper part shows the total eddy kinetic energy for the reference simulation (solid) and for obervations (dashed). The lower part shows the transient eddy kinetic energy.

the transient part (lower part). The values obtained from the model are compared with observed values given by Oort and Peixoto (1983) as mean values of December, January and February for the 1968–1973 period. From the figure, it is seen that except in the equatorial area, the transient eddy energy is somewhat too small, especially in the areas of the westerlies on the northern hemisphere. Moreover it is seen from the figure that the amplitudes of the stationary waves are somewhat too large around 30° N.

The spectral distribution of the kinetic energy must be considered as a fundamental characteristic of the atmospheric circulations in the different horizontal scales. The mean value over the sphere of the kinetic energy K of the rotational part of the flow is written as the sum

$$K = \sum_{m,n} K_{m,n},$$

where $K_{m,n}$ is the kinetic energy of the motion described by the component $\psi_{m,n}$ of the spherical harmonic analysis of the streamfunction ψ. A simplified picture of the spectral energy distribution is obtained by considering the one-dimensional spectra defined by

$$K = \sum_m K_m \quad \text{or} \quad K = \sum_n K_n,$$

where K_m is the sum of energy of all components having the same zonal wavenumber m, and similarly K_n is the sum of the energy of all components with the same spherical harmonic index n. The one-dimensional spectrum K_m is shown in Fig. 11 for the reference simulation as well as for the observed values. It is seen that for the waves with wavenumbers larger than 7, there is very good agreement between simulated and observed values, whereas the simulated energy values are somewhat too small for the long stationary waves ($m = 1$–3) as well as for the dominant baroclinic waves ($m = 4$–7). In a similar way, Fig. 12 shows the simulated and observed spectra K_n with the contributions from the mean zonal flow included. From the spectral representation, it is seen that the smaller values of the simulated kinetic energy in relation to the observed value occur for the components with the values of n in the range from 5 to 10, i.e., components in the two-dimensional representation being an essential part of the stationary waves as well as the main baroclinic waves.

The question about the form of the energy-spectrum has been studied quite extensively during the last 20 years both from analysis of observational data as well as from theoretical considerations. A recent account of the problem representing both the empirical and the theoretical part is given by Boer and Shepherd (1983). From the observations as well as from theory, it is generally agreed that in a certain inertial subrange, the energy-spectrum will decrease approximately in accordance with a -3 power law. So in Figs. 11, 12, the straight lines

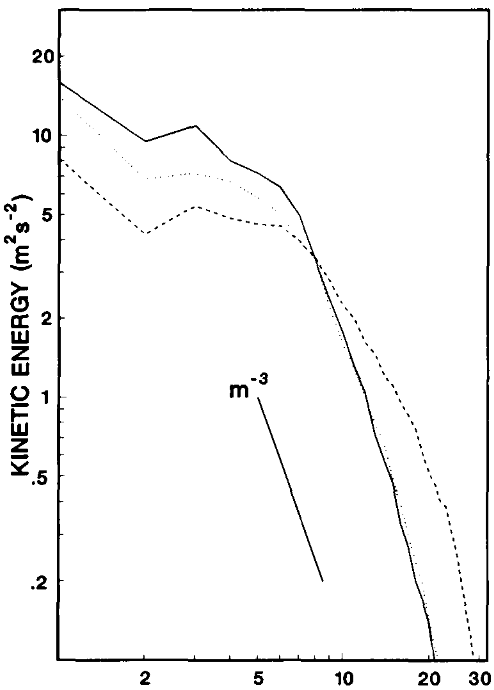

Fig. 11. The spectrum K_m ($m^2\,s^{-2}$) at the 500 hPa level for January 1983 (solid), the reference experiment (dotted) and for the experiment without lateral diffusion (dashed).

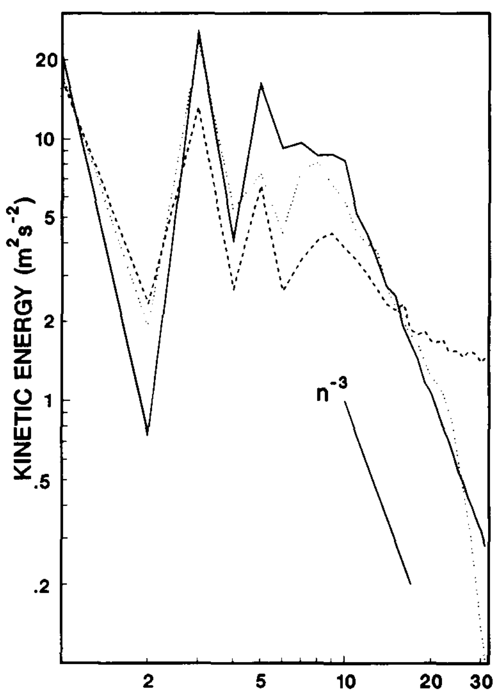

Fig. 12. As Fig. 10, but for the spectrum K_n.

represents the power law m^{-3} and n^{-3}, respectively. For the reference simulation (as for the observed values), it is seen that the K_m spectrum follows the m^{-3} variations quite well for $m > 6$, whereas the K_n spectrum varies as n^{-3} for $n > 10$.

It is to be expected that the eddy kinetic energy and especially its spectral distribution will be influenced strongly by the choice of lateral diffusion. In order to examine this influence, a series of numerical experiments have been carried out with varying strength and scale-dependency of the linear diffusion. The experiments are listed in Table 2. In the B-experiments, the ∇^4 diffusion is used as given by eq. (5), whereas the more scale-selective diffusion given by eqs. (6) and (7) are used in the C-experiments. In both cases, the diffusion represents an exponential damping for each scale represented by n, and in the last column of Table 2, the e-folding decay times for the smallest scale with $n = 31$ are given for the values of the diffusion constants J and L. The experiment C2 is identical to the reference simulation. The results of the experiments may be summarized as in Table 3, giving values of kinetic energy for the larger scale eddies $(KE)_L$ with $n < 19$ and for the rest of the spectrum $(KE)_S$. KT denotes the total kinetic energy. The observed values in the last row are mean values for the three January months of 1983–1985.

By comparing the values from the integration A without any lateral diffusion and the values from the B-experiments, it is seen that the use of ∇^4 diffusion causes a decreasing amount of eddy energy on the smaller scales, $(KE)_S$, and furthermore that this decrease is connected with an increase of the eddy kinetic energy of the larger scales $(KE)_L$. It is seen that the total eddy kinetic energy decreases with increasing strength of the ∇^4 diffusion, and furthermore, that the reduced eddy activity is accompanied by a considerable increase of the kinetic energy of the mean zonal flow and thereby also by an increase of the total kinetic energy. For the more scale-selective diffusion used in C-integrations, this effect of the lateral diffusion is even more pronounced, in the way that the increase of $(KE)_L$ is larger than the decrease of $(KE)_S$, so that the total eddy kinetic energy increases with increasing strength of lateral diffusion. The variations of kinetic energy values shown in Table 3 are quite representative for the whole troposphere with a larger deviation from observed values in the upper part of the troposphere as can be seen from Table 4 showing the values corresponding to Table 3 for the 250 hPa level.

Table 2. *Diffusion experiments*

Experiment	Diffusion coefficient	e-folding decay time in days
A	none	—
B1	$J = 2 \cdot 10^{15}\ m^4\ s^{-1}$	9.68
B2	$J = 10 \cdot 10^{15}\ m^4\ s^{-1}$	1.94
B3	$J = 80 \cdot 10^{15}\ m^4\ s^{-1}$	0.24
C1	$L = 2.5 \cdot 10^{-4}\ s^{-1}$	0.70
C2 (ref.)	$L = 5.0 \cdot 10^{-4}\ s^{-1}$	0.35
C3	$L = 10.0 \cdot 10^{-4}\ s^{-1}$	0.17

Table 3. *Kinetic energy at 500 hPa* ($m^2\ s^{-2}$)

Experiment	$(KE)_L$	$(KE)_S$	KE	KZ	KT
A	34.7	21.0	55.7	41.2	96.9
B1	37.7	17.2	54.9	44.9	99.8
B2	42.2	10.7	53.9	49.8	102.7
B3	43.3	3.0	46.3	62.0	108.3
C1	47.0	11.0	58.0	53.4	111.4
C2 (ref.)	50.8	9.6	60.4	54.9	115.3
C3	53.8	9.2	63.0	56.1	119.1
observed	66.5	9.3	75.7	67.5	143.2

Table 4. *Kinetic energy at 250 hPa* ($m^2\ s^{-2}$)

Experiment	$(KE)_L$	$(KE)_S$	KE	KZ	KT
A	71.3	31.0	102.3	133.7	236.0
B1	76.7	24.6	104.3	139.6	240.9
B2	83.3	12.8	96.1	146.4	242.5
B3	91.9	2.9	94.8	175.4	270.2
C1	91.5	13.2	104.7	153.7	257.4
C2 (ref.)	99.3	11.1	110.4	155.2	265.7
C3	101.5	10.1	111.6	158.4	270.0
observed	149.9	16.4	166.3	210.2	376.5

The effect of lateral diffusion may also be seen from the one-dimensional spectra K_m and K_n. Besides the zonal wavenumber spectra from observations and from the reference integration, Figs. 11, 12 also show the spectrum from the integration without lateral diffusion. The curves in Fig. 11 show clearly the decrease of kinetic energy of the eddies with $m > 8$ and the energy increase for the long waves with $m < 8$ caused by the use of lateral diffusion. Similarly, it is seen from Fig. 12 that the use of lateral diffusion implies in the n-spectrum a drop of energy on the small scales with $n > 15$ and an essential growth of energy on the large scale with $n < 15$.

The linear 4th-order diffusion as given by eq. (5) is quite generally used in spectral models. Thus, it is used in the ECMWF operational model and it was also used in the application of an ECMWF T21 for long-term integrations (Volmer et al., 1984) and for the el Niño anomaly studies by Cubasch (1985). In these studies, the same value of the diffusion coefficient was used as in experiment B1. Actually, this value represents a rather weak diffusion with an exponential e-folding decay time of 44.6 days for $n = 21$. The distribution of eddy kinetic energy with the zonal wavenumber obtained in experiment B1 is shown in Fig. 13. By comparing with the corresponding spectrum from observations, it is seen that spectral blocking with high energy values at the smallest scales is still significant, and actually the spectrum for the B1 integration is quite close to the spectrum from the experiment with no lateral diffusion as shown in Fig. 11. The effect of increasing the value of the diffusion coefficient J in the ∇^4 diffusion is clearly demonstrated in Fig. 13 by the spectral curve resulting from the integration B3 with the large value of $J = 80 \cdot 10^{15}$ $m^4 s^{-1}$. A value of J a little larger than that used in experiment B2 will bring the energy spectrum quite close to the observed spectrum for $m > 6$, but for the larger scales with $m < 6$, the energy will be somewhat smaller than that obtained in the reference simulation.

As the long-term mean flow is strongly influenced by interactions with the eddy motion, it is to be expected that changes of the eddy kinetic energy as well as its spectral distribution connected with changes of the lateral diffusion, must also generate changes of the long-term mean flow. Thus, it is seen from Tables 3, 4 that the

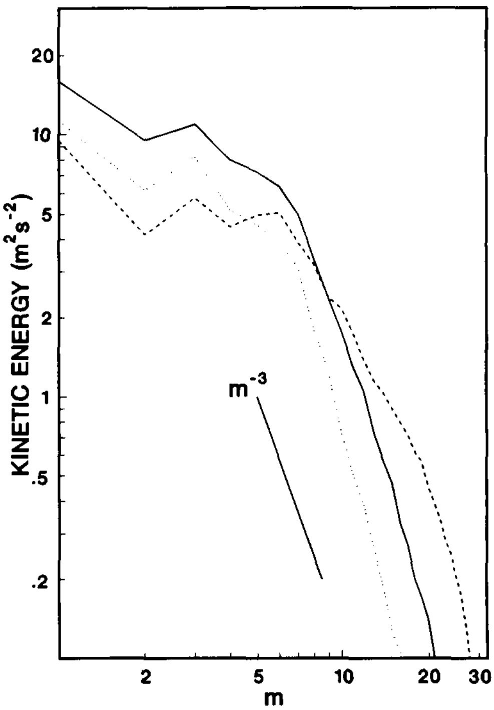

Fig. 13. The spectrum K_m ($m^2 s^{-2}$) at the 500 hPa level for January 1983 (solid), experiment B1 (dashed) and experiment B3 (dotted).

inclusion of lateral diffusion results in all cases in a significant increase of the kinetic energy of the zonal flow. By comparing the mean zonal flow of the experiment without lateral diffusion with the mean flow of the reference experiment, it is found that the use of lateral diffusion results in a considerable increase of the mean zonal velocity in the area from 45°S to 65°S and a smaller but more broadly distributed increase in the region from 25°N to 65°N. Furthermore, the horizontal mean fields are essentially influenced by variations of the lateral diffusion. Considering, for instance, the long-term mean height field of the 1000 hPa surface over the northern hemisphere for the simulation without lateral diffusion, it is found that the low- and high-pressure areas are essentially weaker than those obtained in the reference experiment. A comparison between the different experiments listed in Table 2 shows that the reference experiment simulates the mean observed height of the 1000 hPa level as well as other pressure levels most closely. It must be considered, however, that this result from the reference simulation is also dependent on the inclusion of gravity wave drag effect as shown in Section 3.

5. Concluding remarks

The development of a medium-resolution general circulation model on the basis of a forecast model from ECMWF has been described. Applying the original version of the model with reduced vertical and horizontal resolution for long-term perpetual January simulations, a substantial climate drift of the model was found. In order to reduce this drift, a number of changes has been made in the parameterization of several physical processes. The introduction of a new convective adjustment scheme, which takes into account both deep and shallow convection, resulted in better simulations of the precipitation patterns and some improvement in the level of kinetic energy. These findings have not been further reported in the present paper, where all simulations described have been performed with a version of the model including this convective scheme as described in Section 2. Another change in the model has been the introduction of a parameterization of orographically exited gravity waves. The inclusion of the effect of these small-scale waves by a simple parameterization turned out to have a large effect on the simulated mean fields. Before the inclusion of this parameterization, the model reproduced a too strong polar night jet and a too deep quasi-stationary low pressure in the North Atlantic which furthermore was shifted towards the northeast. These large systematic errors have been considerably reduced after the gravity wave drag parameterization was implemented in the model. These results are in general accorance with those demonstrated in several other models in recent years.

A main problem with the adaption of a high-resolution forecast model in order to make it feasible as a climate model concerns the treatment of the effect of the unresolved scales on the larger scales explicitly described by the model. Conventionally, this influence is parameterized by a linear lateral diffusion term, and two formulations with quite different scale-dependencies have been considered in the present model. A number of experiments with different values for the diffusion-constants have been carried out in order to investigate the effect of this parameterization. It should be noted that in the present model, the same formulation and constants have been applied for all prognostic variables at all levels. The formulation has furthermore been applied and tested on sigma surfaces only. The effect of the formulation and strength of lateral diffusion on the simulated mean fields is of considerable magnitude. It was found that a formulation acting exclusively on the smaller scales is generally the best. The simulated kinetic energy spectrum is, with this formulation, in good accordance with that observed for the medium and smaller scales. Furthermore, an essential improvement in the simulated level of eddy kinetic energy on the larger scales was obtained with this formulation compared with the more commoly used ∇^4 diffusion. This peculiar effect of using the lateral diffusion exclusively on the smaller scales seems to be of quite general nature and not due to any special feature of the model, as for instance the treatment of lateral diffusion on sigma-surfaces, which may be questionable, especially in mountain areas. In any case, quite the same effect of the lateral diffusion formulation was found from numerical experiments with the very simple general circulation model used by Eliasen (1982), i.e., a two-layer primitive equation model with a homogeneous surface.

In contrast to the effect of lateral diffusion, it turns out that the effect on the 90-day mean statistics of the vertical diffusion used is of minor importance. In the present study, the development of individual synoptic systems has not been examined in much detail and the development of individual systems may well be more sensitive to the parameterization of vertical diffusion than gross statistics.

Even with the changes introduced, the model exhibits a significant climate drift with a too low level of eddy kinetic energy and too small variability, especially at low frequencies. Nevertheless, models like this are generally considered as useful tools for studies of principal climatic features related to the general circulation of the atmosphere, such as the atmospheric response to external changes. In the past decade, a good deal of attention and work has been devoted to studies of the appearance and the mechanisms determining the interannual variability of the global climate. The internal variability of the atmosphere alone seems to be too small to explain the observed variability, but without much doubt, the coupled atmosphere-ocean system will contain a large part of the interannual variability. The aim in order to model this variability is to develop fully interactive atmosphere-ocean models. Such models, however, are still in their infancy and furthermore the demand for computer resources necessary in order to use such models is very large. Thus, it seems appropriate to continue the experimentation with general circulation models of the atmosphere with specified lower boundary conditions over the oceans. The impact of anomalous sea surface temperatures on the atmospheric circulation has been studied extensively in recent years. Experimentation with anomalous sea surface temperatures in the tropics has been initiated with the present model and will be followed by experiments concerning the impact of extratropical anomalous sea surface temperatures on the simulated climate.

6. Acknowledgements

The authors gratefully acknowledge ECMWF for generously providing the original model. We also want to thank the Danish Meteorological Institute for the large amount of computer resources made available for this research. The computer time for the longer integrations was provided by UNI*C, Denmark, in connection with the installation of the AMDAHL VP1100.

REFERENCES

Baede, A. P. M., Jarraud, M. and Cubasch, U. 1979. Adiabatic formulation and organization of ECMWF's spectral model. *ECMWF Technical Report No. 15*, 40 pp.

Betts, A. K. 1986. A new convective adjustment scheme. Part I: Observational and theoretical basis. *Quart. J. R. Met. Soc. 112*, 677–691.

Betts, A. K. and Miller, M. J. 1986. A new convective adjustment scheme. Part II: Single column tests using GATE wave, BOMEX, ATEX and arctic air-mass data sets. *Quart. J. R. Met. Soc. 112*, 693–709.

Blackadar, A. K. 1962. The vertical distribution of wind and turbulent exchange in a neutral atmosphere. *J. Geophys. Res. 67*, 3095–3102.

Blackmon, M. L., Mullen, S. L. and Bates, G. T. 1986. The climatology of blocking events in a perpetual January simulation of a spectral circulation model. *J. Atmos. Sci. 41*, 1379–1405.

Boer, G. J. and Shepherd, T. G. 1983. Large-scale two-dimensional turbulence in the atmosphere. *J. Atmos. Sci. 40*, 164–184.

Boer, G. J., McFarlane, N. A., Laprise, R., Henderson, J. D. and Blanchet, J.-P. 1984. The Canadian climate centre spectral atmospheric general circulation model. *Atmosphere-Ocean 22*, 397–429.

Boville, B. A. 1984. The influence of the polar night jet on the tropospheric circulation in a GCM. *J. Atmos. Sci. 41*, 1132–1142.

Charnock, H. 1955. Wind stress on a water surface. *Quart. J. Roy. Met. Soc. 81*, 639–640.

Chen, T.-C. and Wiin-Nielsen, A. 1978. Nonlinear cascades of atmospheric energy and enstrophy in a two-dimensional spectral index. *Tellus 30*, 313–322.

Cubasch, U. 1985. The mean response of the ECMWF global model to the El Niño anomaly in extended range prediction experiments. *Atmosphere-Ocean 23*, 43–66.

Dickinson, A. 1985. The impact of some parameterizations on the UK Meteorological office's forecast models. *Proceedings of ECMWF seminar on Physical Parameterizations*, 9–13 September 1985, Vol. 2, 251–276.

Eliasen, E. 1982. Climate modeling using an equivalent meridional circulation. *Tellus 34*, 228–244.

Eliasen, E., Machenhauer, B. and Rasmussen, E. 1970. On a numerical method for integrations of the hydrodynamical equations with a spectral representation of the horizontal fields. Report. No. 2, Institute of Theoretical Meteorology, University of Copenhagen, Denmark, 37 pp.

Fischer, G., ed. 1987. *Climate simulations with the ECMWF T21-model in Hamburg*. Report No. 1, Meteorologischer Institut, University of Hamburg, Federal Republic of Germany, 159 pp.

Geleyn, J.-F. and Hollingsworth, A. 1979. An economical analytical method for the computation of the interaction between scattering and line absorption of radiation. *Beitr. Phys. Atmos. 52*, 1–16.

Jarraud, M., Simmons, A. J. and Kanamitsu, M. 1985. Impact of an envelope orography in the ECMWF model. *Proceedings of ECMWF seminar on Physical Parameterizations*, 9–13 September 1985, Vol. 2, 199–249.

Leith, C. E. 1971. Atmospheric predictability and two-dimensional turbulence. *J. Atmos. Sci. 28*, 145–161.

Lilly, D. K. 1972. Wave momentum flux-a GARP problem. *Bull. Am. Met. Soc. 53*, 17–23.

Louis, J.-F. 1979. A parametric model of vertical eddy fluxes in the atmosphere. *Boundary-layer Meteorol. 17*, 187–202.

MacVean, M. K. 1983. The effect of horizontal diffusion on baroclinic development in a spectral model. *Quart. J. R. Met. Soc. 109*, 771–783.

Oort, A. H. and Peixoto, J. P. 1983. Global angular momentum and energy balance requirements from observations. *Advances in Geophysics 25*, 355–490.

Orszag, S. A. 1970. Transform method for calculation of vector coupled sums: applications to the spectral form of the vorticity equation. *J. Atmos. Sci. 27*, 890–895.

Palmer, T. N., Shutts, G. J. and Swinbank, R. 1986. Alleviation of a systematic westerly bias in general circulation and numerical weather prediction models through an orographic gravity wave drag parameterization. *Quart. J. R. Met. Soc. 112*, 1001–1039.

Pitcher, E. J., Malone, R. C., Ramanathan, V., Blackmon, M. L., Pain, K. and Bourke, W. 1983. January and July simulations with a spectral general circulation model. *J. Atmos. Sci. 36*, 1498–1529.

Ramanathan, V., Pitcher, E. J., Malone, R. C. and Blackmon, M. L. 1983. The response of a general circulation model to refinements in radiative processes. *J. Atmos. Sci. 40*, 605–630.

Simmons, A. J. and Bengtsson, L. 1984. Atmospheric general circulation models: their design and use for climate studies. In: *The global climate* (ed. J. T. Houghton). Cambridge: University Press, 37–56.

Tiedtke, M. 1985. Effect of physical parameterization on the large-scale flow in the ECMWF model. *Proceedings of ECMWF seminar on Physical Parameterizations*, 9–13 September 1985, Vol. 2, 277–314.

Tiedtke, M., Geleyn, J.-F., Hollingsworth, A. and Louis, J.-F. 1979. ECMWF model parameterizations of sub-gridscale processes. *ECMWF Tech. Report No. 10*, 46 pp.

Volmer, J. P., Deque, M. and Rousselt, D. 1984. EOF analysis of 500 mb geopotential: A comparison between simulation and reality. *Tellus 36A*, 336–347.

Wallace, J. M., Tibaldi, S. and Simmons, A. J. 1983. Reduction of systematic errors in the ECMWF model through the introduction of an envelope orography. *Quart. J. R. Met. Soc. 109*, 683–718.

Zwiers, F. W. and Boer, G. J. 1987. A comparison of climates simulated by a general circulation model when run in the annual and perpetual modes. *Mon. Wea. Rev. 115*, 2626–2644.